The International Society of Precision Agriculture presents the
15th International Conference on
Precision Agriculture
26–29 JUNE 2022
Minneapolis Marriott City Center | Minneapolis, Minnesota USA

Investigation and Development of Automated Analysis of Snowmelt from Time-series Sentinel 2 Imagery to Determine Variable Rate Irrigation Zones in the American Mountain West

Ian Turner[1], Ruth Kerry[1], Ryan Jensen[1], Elisa Woolley[2], Jeff Svedin[3], Neil Hansen[1], Bryan Hopkins[1]

[1]Brigham Young University, USA, [2]Utah State University, USA,
[3]University of Missouri-Columbia, USA.

A paper from the Proceedings of the
15th International Conference on Precision Agriculture
June 26-29, 2022
Minneapolis, Minnesota, United States

Abstract.

The American West is currently experiencing a “mega drought”. Variable rate irrigation (VRI) of crops is a promising approach for saving water whilst maintaining crop yields in this semi-arid region. Southern Idaho, is one of the main agricultural areas in the American Mountain West. Annual precipitation levels are typically <500 mm with most falling as winter snow or spring rain and it has been suggested that snow accumulation and melting patterns influence soil moisture at the beginning of the season. This research investigates whether snow melt patterns measured using time-series Sentinel 2 imagery in Google Earth Engine can be used as to define VRI management zones that are not labor intensive or expensive to produce. The study focuses on two field sites in Southern Idaho where intensive soil, plant and topography related data have been collected to evaluate the approach. The Normalized Difference Snow Index (NDSI) was computed for each 10 m pixel per field that had some snow in it. The NDSI values were ranked and average ranks calculated for each month and over several years. NDSI based zones were calculated on the mean ranks of March NDSI. They showed consistent and significant differences between zones in terms of most of the soil, plant and topographic variables examined. These differences were more consistent in their order of magnitude than those for VRI zones which were calculated based on data that are more labor intensive to collect. The code for automated extraction of appropriate NDSI data from Google Earth Engine is presented making this approach easily transferable to other locations where snow is a primary source of soil moisture.

Keywords.
Normalized Difference Snow Index, Sentinel 2 Imagery, Variable Rate Irrigation, Management Zones.

Introduction

Variable rate irrigation of crops is a promising approach for saving water whilst maintaining crop yields in the semi-arid American Mountain West – much of which is currently experiencing a "mega drought". However, to achieve the potential of a VRI system, accurate irrigation management zones must be identified within fields (Khosla et al., 2008; O'Shaughnessy et al. 2019). The first step in determining irrigation zones involves characterizing the patterns of spatial variation in soil moisture and other key variables like crop yield, topography and soil texture etc. and determining if these patterns are relatively stable temporally. Characterizing variable rate irrigation (VRI) zones is usually done with ancillary data that is likely to be related to the variations in soil moisture and these other key variables. Once zones are defined, soil moisture sensors are usually installed in each zone. Very little is usually known about the degree of variation in soil moisture within the zones or in the field in general away from the soil sensor locations. Accurately, mapping soil moisture levels involves expensive and time-consuming field and lab work and the ultimate goal with VRI is to influence yield which is influenced by other factors in addition to soil moisture.

In Southern Idaho, one of the main agricultural areas in the American Mountain West, annual precipitation levels are typically < 500 mm with most falling as winter snow or spring rain. Svedin et al. (2021) note that in such locations winter snowfall and spring thaw act as the principal wetting event and that the variation of water content at spring green-up seems to be a function of snow accumulation and melting patterns over the winter and early spring. A logical extension of this is that snow accumulation and melting patterns are likely to be related to micro-topographic features such as aspect which influences the amount of insolation received at each location and in turn will influence the water needs of the crop during the season and the likely yield.

This research develops code to automatically extract time-series Sentinel 2 imagery from Google Earth Engine and calculate and analyze patterns in the Normalized Difference Snow Index (NSDI). The term NDSI was first used by Hall et al. (1995) but similar methods had been used to map and separate snow from clouds since the mid-1970s (Hall and Riggs, 2007). Most studies have used the NDSI calculated from different satellite remote sensing products to monitor snow cover in mountainous areas to infer variability in the water supply and increased melting rates associated with global warming (Lin et al., 2012, Nagajothi et al. 2019, Sharma et al. 2012 and Zhang et al. 2021). It has also been used to monitor how pollutants landing on the snow surface alter the albedo effect of the snow (Dozier et al. 2009) and to estimate snow cover in forested areas (Shimamura et al. 2006). However, to our knowledge, the NDSI has not been used to predict levels of soil moisture in an agricultural context.

This paper examines if VRI zones developed from March average ranks of NSDI across several years show significant differences in spring soil moisture and other key variables like yield, aspect etc. The study focuses on two field sites in Southern Idaho. Dense soil sampling followed by laboratory determination of soil moisture content and other related variables has been undertaken at both sites to allow accurate geostatistical mapping of soil moisture patterns in the fields. Yield data were also collected along with a digital elevation model (DEM) from the global positioning system (GPS) attached to the yield monitor. All of these variables are compared between zones developed using NDSI and zones used by Woolley et al. (2021) in one of the fields. The zones of Woolley et al. (2021) were developed using the soil moisture and other data using a more labor and computationally involved approach. Smith et al. (2021) reviewed approaches that have been used for developing VRI zones and advocated approaches based on various wavebands from satellite remote sensing products. To our knowledge analysis of snowmelt patterns using satellite remote sensing has not previously been investigated for the purposes of precision agriculture or precision irrigation.

Methods

Field Sites and Data Collection

Data were collected at two arable field sites in Southern Idaho, USA that had central pivot irrigation systems installed. The first site, which forms the main focus of this study, was located near Grace, Idaho (elevation 1687 m above sea level; 42.60904 latitude and -111.788 longitude) Woolley et al. (2021). It is a 22 ha semi-circular agricultural field covering the northern half of a central pivot. The southern part of the central pivot is a golf course. A wheat-wheat-potato crop rotation is employed in the field. The soil series is Rexburg-Ririe complex with 1 to 4 % slopes and has a consistent silty clay loam texture throughout the field. The climate of southern Idaho, a semi-arid region, is typified by relatively hot days and cool nights during the summer growing season. Average annual precipitation is 390 mm with the majority occurring as winter snow, which often blows and accumulates variably based on topography and surface soil tillage/plant residue (Woolley et al, 2021). The variation of elevation within the field (Fig. 1b) shows only about 7 m difference in the highest and lowest elevation locations, but a key feature of the elevation patterns is a west-facing slope which bi-sects the middle of the field.

The Grace field was studied in the 2016-2021 growing seasons. During that time the crops were: 2016 – wheat, 2017 – wheat, 2018 – potato, 2019 – wheat, 2020 – wheat and 2021 – potato. Wheat yield data were collected using a mass-based yield sensor equipped with a GPS located on the combine. Yield data were pre-processed before mapping to remove artefacts related to double passes of the combine over certain areas etc. A DEM was developed from the elevations associated with the GPS locations from yield monitoring. Saga GIS was used to compute derived topographic attributes such as aspect, slope and topographic wetness index (TWI) from the DEM. During the 6 growing seasons 85-102 soil samples were collected throughout the field (Figure 1a). For the earlier seasons, samples were collected in Spring and Fall, but samples were collected up to four times in later growing seasons. Soil samples were collected at four depths (0-0.3 m, 0.3-0.6 m, 0.6-0.9 m, and 0.9-1.2 m) using a modified gas-powered post driver (AMS, Inc. American Falls, ID, USA). Gravimetric water content of the soil was determined by drying in a forced air oven at 105^{o}C until consistent weights were reached. Gravimetric water contents were converted to VWC using soil bulk density values determined in 2016 (Svedin et al., 2021). Evapotranspiration (ET) levels were modelled at different times using the American Society of Civil Engineers FAO Penman-Monteith equation (Allen et al. 1998).

Irrigation zones (Woolley et al., 2021) were developed in 2019 by analyzing patterns in 2016 and 2017 crop water productivity (CWP), which is calculated from yield and ET data. This was accomplished by using a regression where yield was the response variable and ET was the explanatory variable. Then, a k-means clustering algorithm with constraints for spatial contiguity was used to map out the five irrigation zones (Woolley et al., 2021). These zones seem to be effective, but they are based on very labor-intensive data collection and analysis. ET calculations were derived from soil moisture measurements from 102 locations at 4 depths taken four times throughout the growing season. These zones, hereafter referred to as the Woolley et al. zones, are shown as the black lines in Figure 1a and were used as a comparison for those developed using automated time-series snow-melt analysis.

The Rexburg field (43.80103 latitude, -111.791956) had soils of four types: the Pocatello variant silt loam, 2 to 4 percent slopes and Pocatello variant silt loam, 4 to 8 percent slopes, the Ririe silt loam, 4 to 8 percent slopes and the Ririe silt loam, 12 to 20 percent slopes (see black lines in Figure 6D). Figure 1d shows about 20 m variation in elevation within the field and the soil type names suggest some rather steep slopes are found in this field. Soil samples in the Rexburg wheat field were collected at 66 locations at the four depths mentioned above, four times in the 2019 growing season (Figure 1c). The same methods were used to determine gravimetric water contents for these samples as were used for the Grace soil samples. Yield data for 2019 were collected and a DEM from the GPS locations of yield measurements used to calculate derived topographic attributes in Saga GIS.

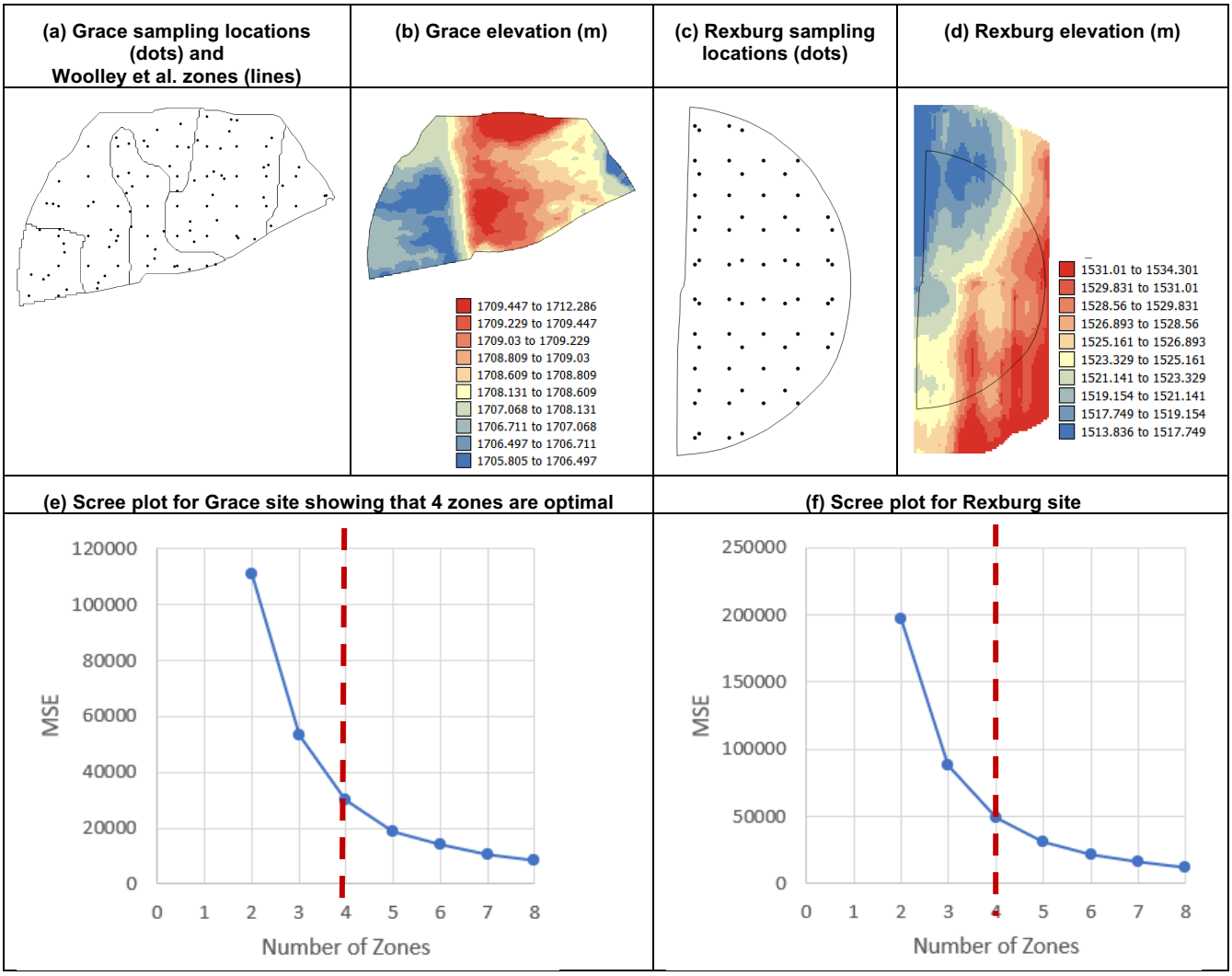

Figure 1. Maps showing the location of sampling points within the (a) Grace and (c) Rexburg fields and elevation for the Grace (b) and Rexburg (d) fields. Scree plots for the Grace (e) and Rexburg fields (f) showing the optimal number of zones

Coding and Development of Automated Image Extraction

Sentinel 2 imagery was chosen for this analysis as it is freely available through Google Earth Engine, has a relatively small 10 m pixel size and it captures suitable wavelengths for calculating the normalized difference snow index (NDSI). The equation for the NDSI is:

$$NDSI = (Green - SWIR\ 1) / (Green + SWIR\ 1) \quad (1)$$

For Sentinel 2, Green = Band 3 and SWIR 1 = Band 11. If NDSI >0, there is snow in that pixel, if it is 0.5, 50% of the pixel is covered in snow and If NDSI = 1, the pixel is completely covered in snow. Sections of the code used to extract images with snow cover for the study sites and calculate the NDSI are shown below.

The code shown in (lines 1-8) calls on two github users' previous work. The spectral package is a database of different indices and their formulae. This was provided by the user "dmlmont" on github. The palettes package is a database of different color ramps. This was provided by the user "gena" on github. The palettes were not required for any actual analysis, but were used to more easily visualize the data on Google Earth Engine. The palette used was "haline", which is a color ramp from navy blue to yellow to green.

```
1  // REQUIRE THE SPECTRAL MODULE
2  var spectral = require("users/dmlmont/spectral:spectral");
3
4  // REQUIRE THE PALETTES MODULE
5  var palettes = require('users/gena/packages:palettes');
6
7  // HALINE PALETTE
8  var haline = palettes.cmocean.Haline[7];
```

The code shown in (lines 10-20) shows how images from Google Earth Engine were selected for a given date range if they had less than 40% clouds, then selected for the agricultural field of interest using a shape file. All of the images for the date range were then overlain and the median values of each band for each pixel were calculated for that date range.

```
10 // DATASET TO USE: SENTINEL-2
11 var dataset = 'COPERNICUS/S2';
12
13 // FILTER THE DATASET by median
14 //Collect Sentinel images, filter by time, and add to map
15 var S2 = ee.ImageCollection('COPERNICUS/S2')
16 .filterDate('2019-03-01', '2019-03-31')
17 .filter(ee.Filter.lt('CLOUDY_PIXEL_PERCENTAGE', 40))
18 .filterBounds(Grace)
19 .median();
20 print('Collection: ', S2);
```

Key for lines 10-20:

Image collection = multiple images combined into one image
Filter date = the date range to pull those images from
Filter lt = exclude images that are over 40% clouds
Filter bounds = region that images must touch
Median = overlay each image and take the median value of each band for each pixel
This is good at removing clouds, ensuring that there are no outliers, and smoothing the image

The code shown in (lines 22-32) checks which bands are required for the NDSI calculation. This prints onto the Google Earth Engine console and searches the spectral package from line 2. The SWIR1 (Band 11) and Green (Band 3) bands are correctly selected, and are inserted as the variable “parameters”. From there, the NDSI is calculated for the entire image, using that same spectral package mentioned in lines 1-8.

```
22 // CHECK THE REQUIRED BANDS FOR NDSI
23 print('Required bands for NDSI',spectral.indices.NDSI.bands);
24
25 // REQUIRED PARAMETERS ACCORDING TO THE REQUIRED BANDS
26 var parameters = {
27   "S1": S2.select("B11"),
28   "G": S2.select("B3")
29 };
30
31 // COMPUTE THE NDSI
32 var S2_NDSI = spectral.computeIndex(S2,"NDSI",parameters);
```

Key for lines 22-32:

Parameters = created variable that represents required bands

The code in lines 34 to 55 starts by clipping the new image with the new NDSI band added. This is done because it is only necessary to examine the study area for the following steps. The NDSI band is then printed to the Google Earth Engine console, and each layer is added to the map. The map is visualized with the haline palette to represent the NDSI band. Then the map is centered over the study area. Finally, the clipped image is downloaded straight to Google Drive in the GEOTIFF file format for further analysis.

```
34  ///CLIP IMAGE
35  var S2clipped = S2_NDSI.clip(Grace);
36
37  // CHECK THE NEW BAND: NDSI
38  print("New band added: NDSI",S2_NDSI);
39
40  // ADD THE NEW BAND TO THE MAP AND TRUE COLOR IMAGE
41  //Map.addLayer(S2_NDSI, {"min":0, "max":1, "bands": ["B4", "B3", "B2"]}, 'True Color Image');
42  Map.addLayer(S2_NDSI,{"min":0,"max":1,"bands":"NDSI","palette":haline},"NDSI");
43  Map.addLayer(S2clipped,{'min':0, 'max':1, 'bands': 'NDSI', 'palette':haline}, 'NDSI Clipped');
44  Map.centerObject(Grace, 15);
45  Map.addLayer(Grace, {color: '#FF0000'}, 'Grace');
46
47  //Export
48  Export.image.toDrive({
49      image: S2clipped,
50      description: 'Mar19',
51      folder: 'GEE',
52    region: Grace,
53      scale: 10,
54      fileFormat: 'GEOTIFF'
55  });
```

Key:

S2clipped = clipped version of image

S2_NDSI = Sentinel image with NDSI band calculated

Each of these images was downloaded and brought to ArcGIS Pro and run through a model to assign points to each pixel using a fishnet. UTM coordinates were assigned to each of the points which had all of the data from the downloaded image. This shapefile was exported and uploaded to SPSS, where each pixel was given a rank based on the NDSI value. Small values were given lower ranks, and larger values were given higher ranks. Tied values were given their mean rank.

Each image with a maximum NDSI value greater than 0.5 was selected for further analysis. These files were merged together to create files with data for the same month in different years. An average rank value was then calculated on ArcGIS Pro by calculating the mean of each year's rank. This was done by month for January, February, and March. Although there were images available from November to March from 2016 to 2022, November did not have any images that had a maximum NDSI value greater than 0.5. December, January, and February each had available data for every year that qualified (except February 2020), however the NDSI values for these months were not indicative of the melting pattern for the end of the season. March had data available for 2020 to 2022 and was generally indicative of the final melting pattern of each season.

Statistical Analysis

Soil, topographic and vegetation variables were all kriged to a 5 m grid to show the spatial patterns in map form. Local averages of 9 points from the 5 m grid were used to assign values of the soil and vegetation variables to the centroids of the 10 m pixels from the Sentinel 2 imagery. Pearson correlation coefficients were calculated between soil, topographic and vegetation variables and monthly averages of NDSI ranks and monthly averages of NDSI ranks from several years.

The March NDSI ranks from several years were classified into 2-8 classes using K-means. A scree plot (Figure 1 e) was used to determine that 4 zones was optimal for the Grace site and a scree plot (Figure 1 f) was used to determine that 4 zones was optimal for the Rexburg site.

Results and Discussion

Figure 2 shows maps of key soil and plant variables at the Grace site for different years. It is clear from these maps that the patterns of several variables correlate negatively with patterns in elevation (Figure 1b), (r = -0.250 to -0.576). The slope that bisects the field is associated with low yield and TWI and the flatter areas above and below this slope have higher yield and topographic wetness values (Figure 2 b and e). It also seems that this west-facing slope (Figure 2f) is associated with elevated ET levels. Spring soil moisture 2016, Yield 2017 and CWP 2019 all show an area with low values around the center of the central pivot in the central southern part of the field, but the patterns of variation in these variables are less consistent with one another for the rest of the field so the correlation coefficients between these variables for the whole field were low (r = -0.48 to 0.127).

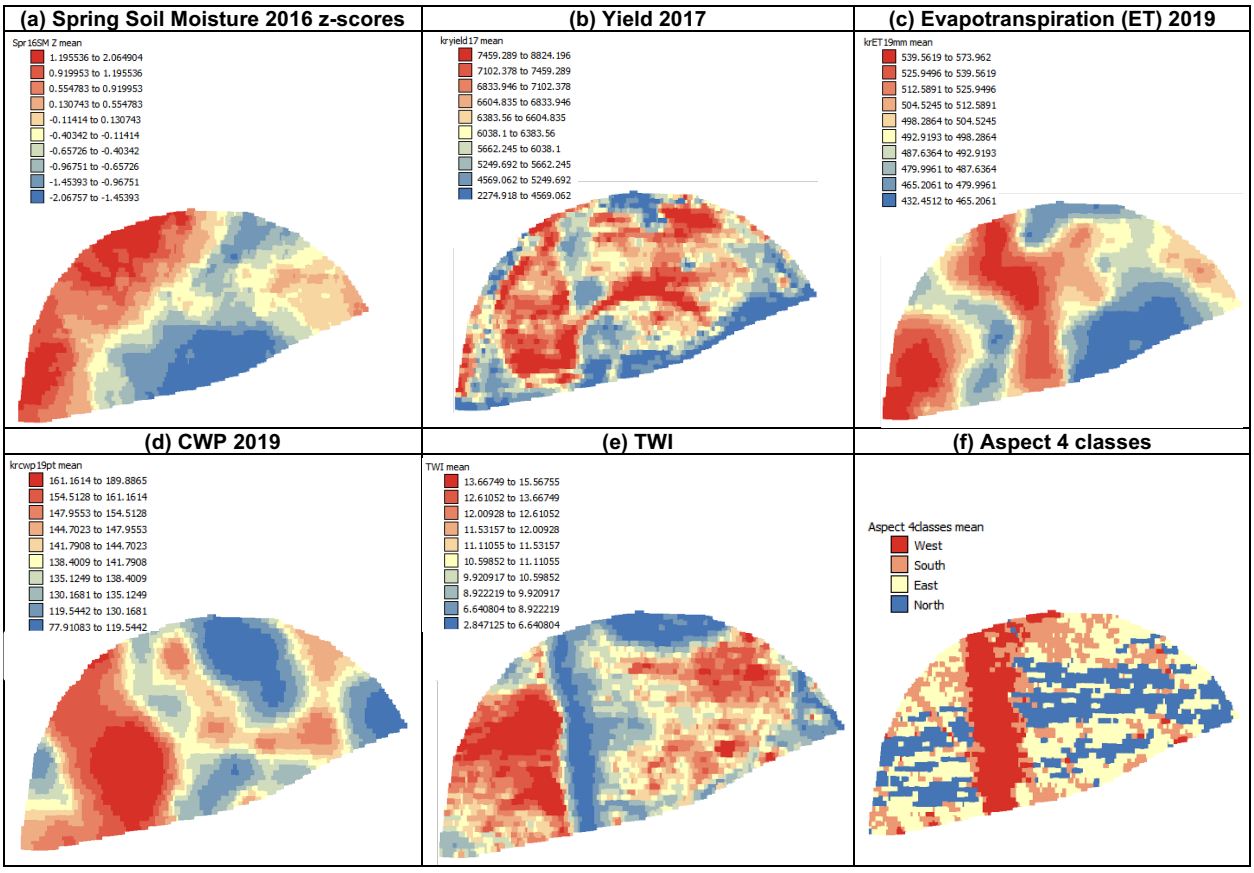

Figure 2. Maps of Key Soil and Plant Variables at the Grace Site from different years (a) Spring soil moisture 2016, (b) Yield 2017, (c) Evapotranspiration 2019, (d) Crop water productivity 2019, (e) Topographic Wetness Index and (f) Aspect

Figure 3 shows the average ranks of NDSI for January, February and March over a series of years and images. The January and February maps (Figure 3a and b) show an area with low ranks in the west of the field in the flat area at the bottom of the slope. This corresponds with an area of high ET, CWP and TWI (see Figure 2 c, d and e, respectively) and correlation coefficients between these variables and February NDSI were generally low at 0.048, -0.200 and -0.422, respectively. The areas of the field with low ranks suggest there is less snow in these areas while some of the highest ranks for January and February, the snowiest months, occur along the slope. This is probably due to winds coming predominantly from the west in Idaho and causing drifts of deeper snow against the slope as suggested by Woolley et al. (2021).

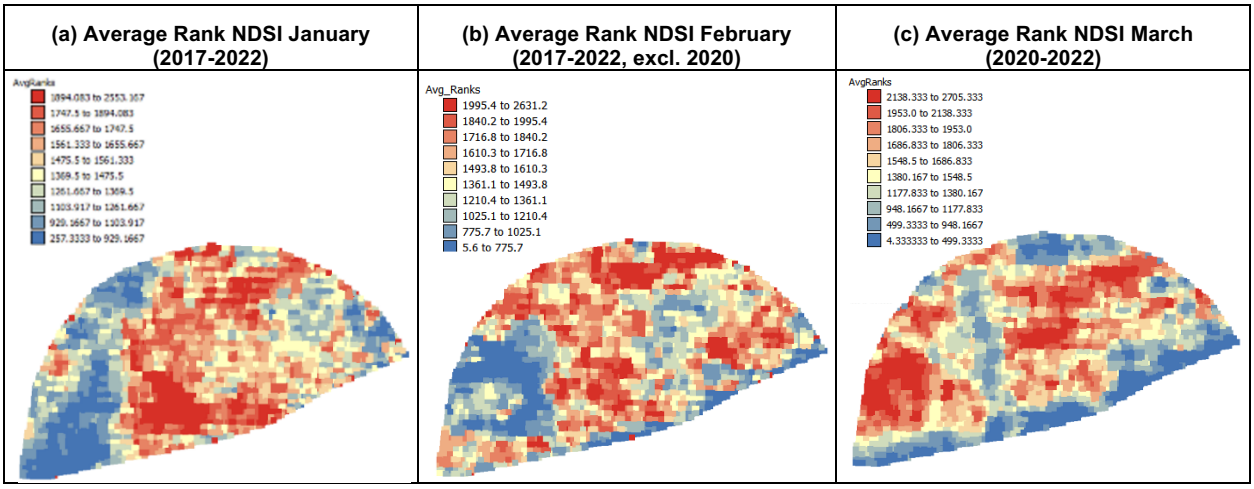

Figure 3. Maps of average rank of NDSI for (a) January 2017-2022, (b) February 2017 to 2022, excluding 2020 and (c) March 2020-2022. *Low ranks indicate less snow coverage and high ranks more snow coverage.*

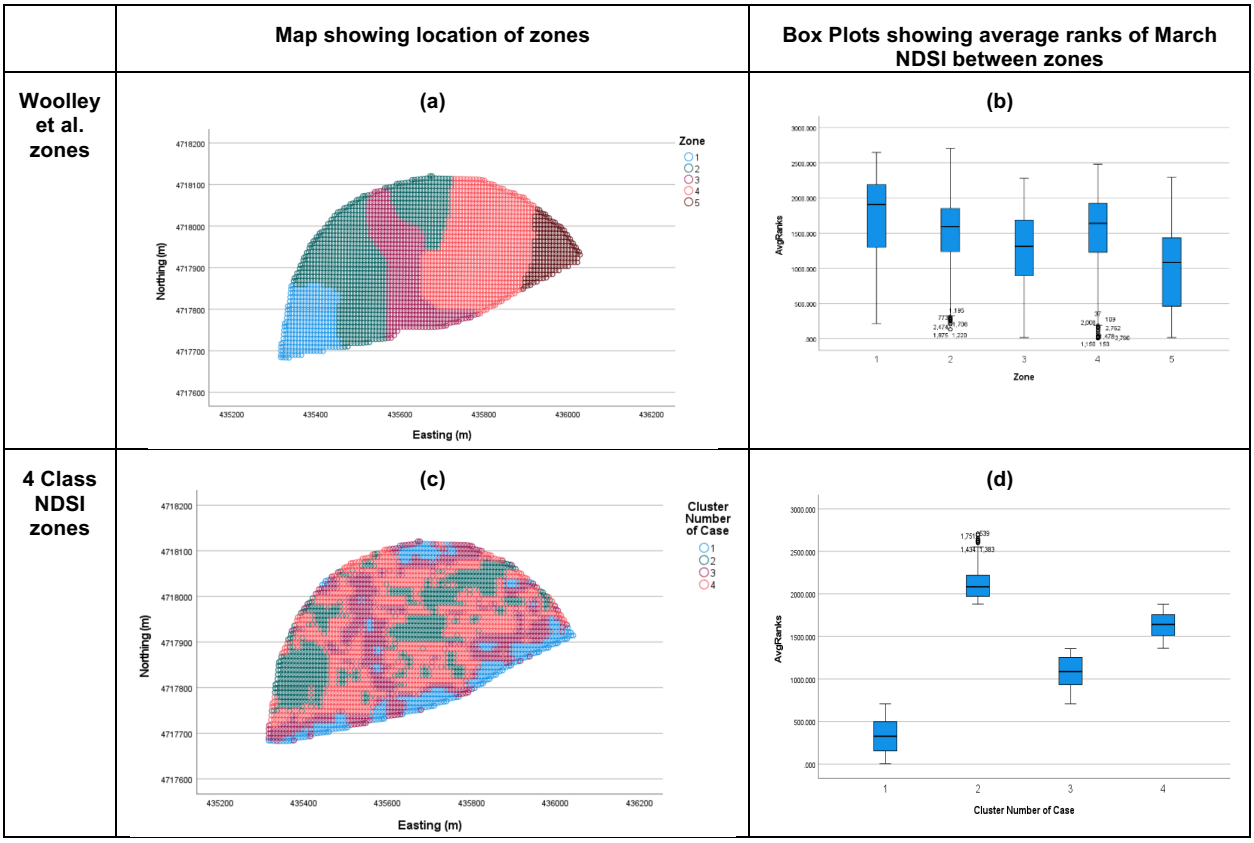

Figure 4. Maps showing location of (a) Woolley et al. zones and (c) 4 class NDSI zones, and Box plots showing the average ranks of March NDSI values for the (b) Woolley et al. zones and (d) the 4 class NDSI zones

Figure 3c, the average ranks for March, shows very similar patterns to yield 2017, TWI and aspect (see Figure 2b, e and f, respectively) and correlation coefficients with these variables were 0.592, 0.481 and -0.304, respectively. These patterns and correlation coefficients show that to characterize the patterns of snow melt in the field, it is best to look at NDSI data from towards the end of the snow season, rather than look at the months when snow can be deep. Average March NDSI ranks are generally highest on north-facing slopes and least on west and south facing areas. This makes sense as north-facing slopes receive less direct sun-light and are generally cooler so snow will melt latest in these areas. As March NDSI ranks had the highest correlations with the variables shown in Figure 2, they were used with K-means to develop a zone classification. The

scree plot in Figure 1e shows that 4 classes was optimal for these data. Figure 4c shows the location of these zones and the boxplot (Figure 4d) shows the significant differences in the the NDSI ranks with very little, if any, overlap in the boxplots for each class. For comparison, Figure 4a shows the location of the zones developed by Woolley et al. with data that were far more labor-intensive to collect. The boxplot, Figure 4b shows the average March NDSI ranks for each of these 5 zones. Although there are clear differences between the classes, there is considerable overlap in the box plots.

Non-parametric Kruskal Wallis H tests were used to compare the values of key soil and plant variables between the Woolley et al. zones and the 4 class NDSI zones (Table 1). These results show that there were highly significant (p<0.001) differences in the values of each of the variables between zones for the Woolley et al. and for the 4 class NDSI zones. However, the zones with the highest and lowest mean ranks were more consistent for the 4 class NDSI zones than for the Woolley et al. zones. Table 1 shows that for the Woolley et al zones, class 1, which is located at the base of the slope (blue areas in Figure 4a) had the highest values of potato yield in 2018, TWI, Spring soil moisture 2016 and ET 2019 (Figure 5 c, e, i and k). The lowest mean ranks for these variables, however, can be found in zone 3 (the slope) for potato yield 2018 and TWI (Figure 5 c and e) and in zone 4 (the flatish plateau area above the slope) for Spring soil moisture 2016 and ET 2019 (Figure 5 i and k).

Table 1. Results from Kruskal Wallis H tests comparing the Woolley et al. classification and the 4 class NDSI zones for different variables

Variable and Date	*Woolley et al. zones*		*4 class NDSI zones*	
	p-value	Classes with highest and lowest mean ranks (eg H-1, L-5)	*p*-value	Classes with highest and lowest mean ranks (eg H-1, L-4)
Yield 2017 (wheat)	<0.001	H-2, L-5	<0.001	H-2, L-1
Yield 2018 (potato)	<0.001	H-1, L-3	<0.001	H-2, L-1
TWI	<0.001	H-1, L-3	<0.001	H-2, L-1
Aspect 4 class	<0.001	H-3, L-5	<0.001	H-3, L-2
Spring soil moisture 2016	<0.001	H-1, L-4	<0.001	H-2, L-1
ET 2019	<0.001	H-1, L-4	<0.001	H-2, L-1
CWP 2019	<0.001	H-2, L-5	<0.001	H-4, L-1

In contrast to the comparison test results for the Woolley et al. zones, the zones with the highest and lowest mean ranks are very consistent for the 4 class NDSI zones. Class 2 has the highest rank for all variables apart from aspect and CWP (Table 1 and Figure 5 h and n). CWP doesn't show much difference between zones (Figure 5n). Class 1 has the lowest rank for all variables apart from aspect. Aspect behaves differently as a variable due to the circular nature of degrees for compass directions – 1-4 are not ordinal but rather arbitrary numbers to signify directions. Bearing this in mind, the aspect of zones is as one might expect given the zones with the highest and lowest ranks of other variable. NDSI zones 1 and 3 had average aspects of 3, equivalent to mostly south-facing slopes, but zone 3 clearly includes some west-facing slopes. This makes sense given that zones 1 and 3 had the lowest average March NDSI ranks (Figure 4d). Zone 2 has the lowest average rank of 2 for aspect corresponding with predominantly north and east facing slopes and the highest mean NDSI values (Figure 4d). This means that although the NDSI zones with the highest and lowest ranks for aspect are different from the other variables, they are actually consistent with the patterns in snow melt and other variables. Zone 2 having the highest rank of most variables and zone 1 having the lowest rank for all variables apart from CWP shows the consistency of these patterns with the classes of March NDSI ranks (Figure 4d). The box plots for yield 2017 – wheat, yield 2018 – potato, TWI, Spring soil moisture 2016 and ET (Figure 5b, f, j and l) all mimic the same order of means shown in the NDSI box plots (Figure 4d) to a greater or lesser degree. The biggest similarities are for TWI, aspect and yield 2017 – wheat. It is interesting, however, that both wheat and potato yield respond similarly to these zones. The strongest relationships with TWI and aspect show that these variables influence snowmelt patterns, and soil moisture, but are also likely to have a strong influence on water use (ET) and

yield as they strongly influence patterns of insolation and the thermal properties at the surface experienced by the crop. The results of comparison tests suggest that the NDSI zones may be more useful than the Woolley et al. zones (Figure 4a), however, the NDSI zones (Figure 4c) are quite fragmented in their distribution. An ideal property of zones for precision agriculture is that they are not spatially fragmented so that it is technically possible to manage them with the available equipment (Tisseyre et al., 2008). This is why the Woolley et al. classification used constraints for spatial contiguity. Such spatial constraints may need to be applied to the NDSI zones in future work.

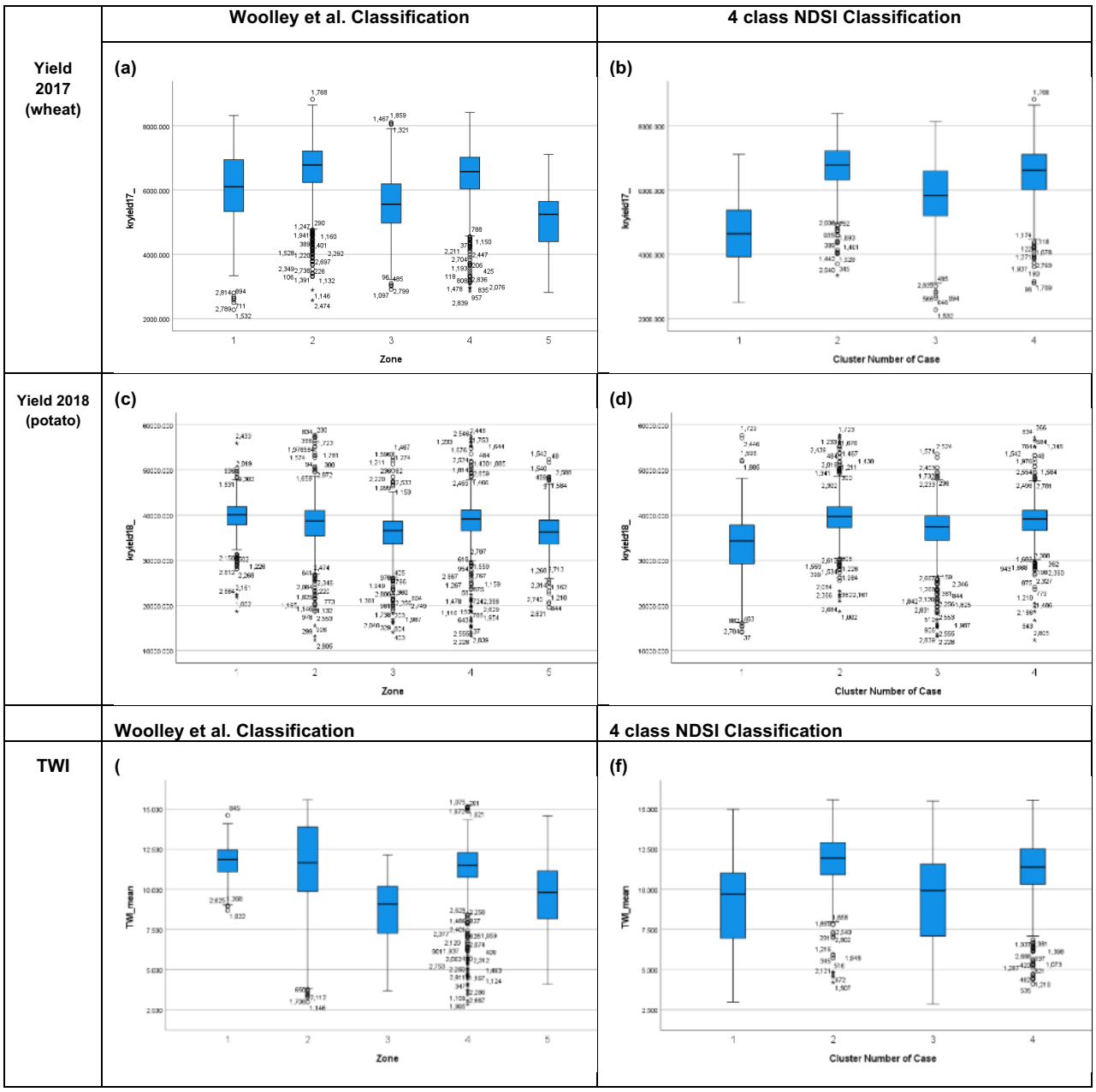

Figure 5. Box plots showing the differences in key variables between zones based on the Woolley et al. (2021) classification and the 4 class NDSI classification

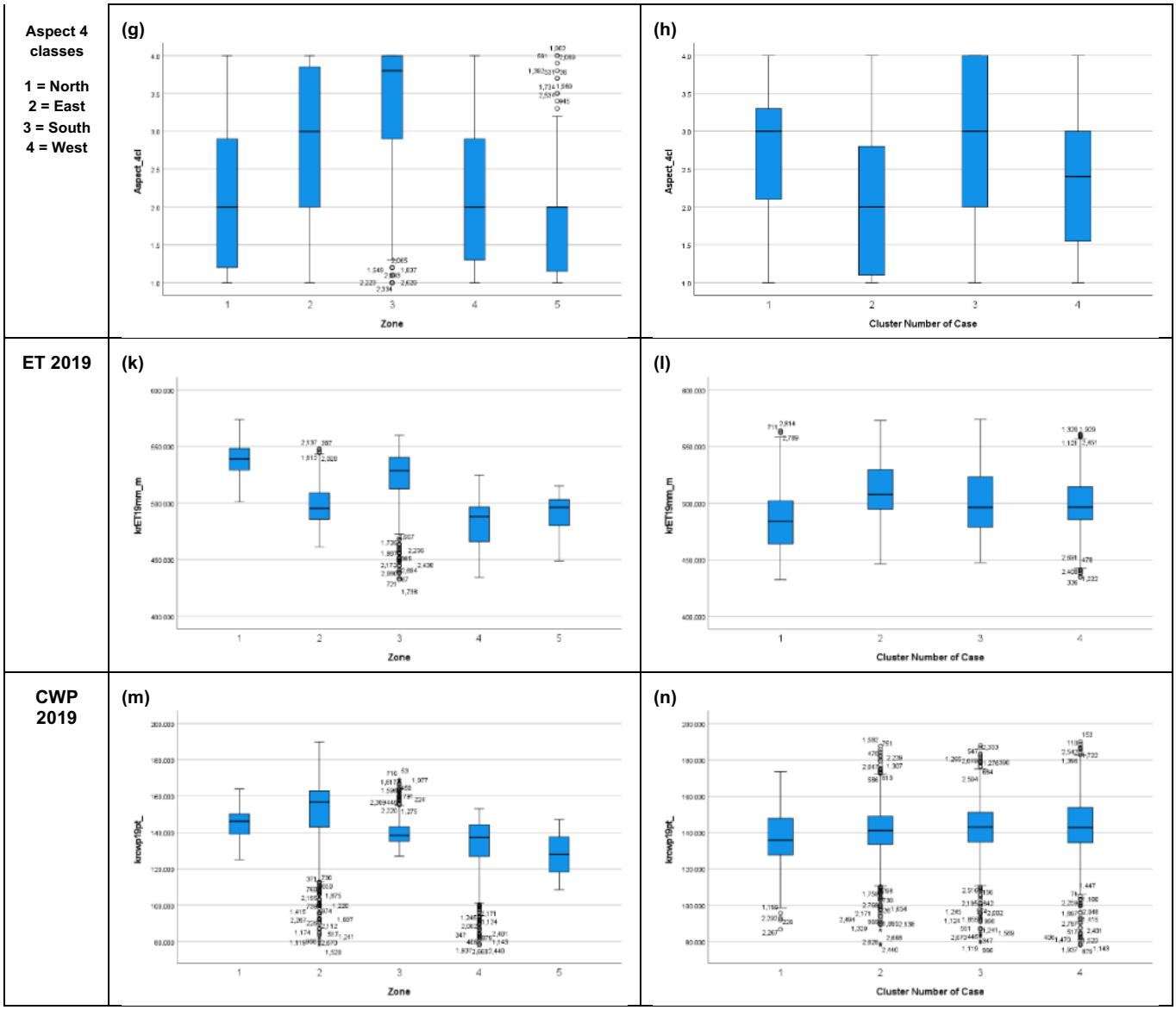

Figure 5. Box plots showing the differences in key variables between zones based on the Woolley et al. (2021) classification and the 4 class NDSI classification continued.

Analysis was done for the Rexburg site just for 2019. Figure 6a shows the average NDSI values for March 2019 and Figure 6b shows the NDSI zones based on these data. Figure 6 c shows that zone 1 had the most snow, followed by zones 4, 3 and zone 2 had the least snow (order of zones 1,4,3,2). Kruskal Wallis H tests suggested highly significant (p<0.001) differences between the NDSI zones for 2019 wheat yield, aspect, TWI, slope and 2019 spring soil moisture. For each variable, the order of mean ranks from the Kruskal Wallis H tests for the zones was: 1,4,3,2, the same as the order for NDSI values. This shows that the zones with the most snow had the largest slope angles, highest TWI values, highest yield and had a greater proportion of north-facing slopes. Figure 6 d and e illustrate this same order of zones as the NDSI ranks for yield and TWI, however, there is far more overlap in the distribution of the box plots for these variables than shown for NDSI in Figure 6c.

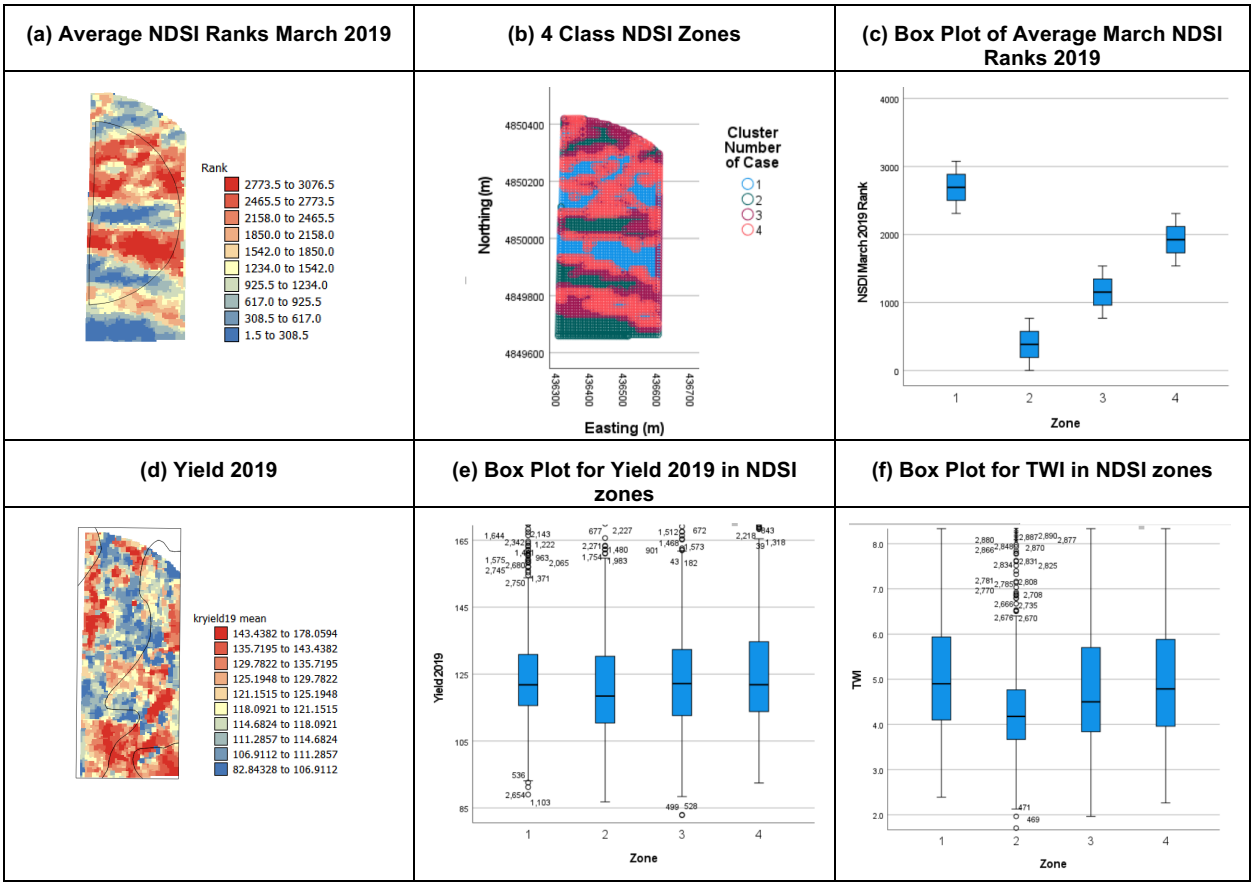

Figure 6. Maps and Boxplots for the Rexburg Site: (a) Map of March Average Rank of NDSI, (b) NSDI zones, (c) Box Plot of Average March NDSI Ranks, (d) Map of Yield 2019, (e) Box Plot of Yield 2019 for NDSI zones and (f) Box Plot of TWI for NDSI zones

Conclusions

Variable rate irrigation zones developed based on the automated extraction of March NDSI data from Sentinel 2 imagery in Google Earth Engine (4 class NDSI zones) show significant differences in several key variables between the zones for the Grace site. There is also a greater consistency in the order of magnitude of these variables with zone than for the Woolley et al. classification which was developed based on data that were far more time and labor-intensive to collect. The NDSI zones showed consistency in the order of magnitude between zones particularly for aspect, TWI and yield data. Given the nature of snowmelt and the likely relationship of these other properties to patterns of insolation it is hypothesized that the zones based on NDSI will be particularly useful for VRI. However, as images with snow cover in March were not available for some years, the importance of calculating an average over several years is hi-lighted.

The results using just one year of data for the Rexburg site suggest that the NDSI zones are similarly useful there but may be more useful when more years of NDSI data are included. Now the code is written, developing NDSI based zones from Sentinel-2 imagery should be a semi-automated process that is easily transferable to other locations in the Mountain West of the USA and other countries and areas where the principal source of soil moisture for crops is snowmelt.

The NDSI zones for Grace were quite fragmented spatially, so future work should focus on adding a spatial constraint to the NDSI zone development to make management of these zones more technically viable with the variable rate central pivot irrigation technology currently available. Future work could also validate the NDSI approach using March snow depth data and analysis of more years of data at the Rexburg site.

References

Allen, R.G. Pereira, L.S. Rae, D. & Smith, M. (1998). Crop Evapotranspiration: Guidelines for Computing Crop Water Requirements. In: FAO Irrigation and Drainage Paper No. 56; Food and Agriculture Organization of the United Nations: Rome, Italy.

Dozier, J., Green, R. O., Nolin, A. W. & Painter, T. H. (2009). Interpretation of snow properties from imaging spectrometry. Remote Sensing of Environment, 113, S25–S37.

Hall, D. K., & Riggs, G. A., (2007). Accuracy assessment of the MODIS snow-cover products. Hydrological Processes, 21, 1534-1547.

Hall, D. K., Riggs, G. A., & Salomonson, V, V., (1995). Development of methods for mapping global snow cover using Moderate Resolution Imaging Spectroradjometer (MODIS) data, Remote Sensing Environment, 54, 127-140.

Khosla, R., Inman, D., Westfall, D. G., Reich, R. M., Frasier, M., Mzuku, M., Koch, B. & Hornung, A. (2008). A synthesis of multi-disciplinary research in precision agriculture: Site-specific management zones in the semi-arid western Great Plains of the USA. Precision Agriculture, 9, 85–100.

Lin, J. T., Feng, X. Z. Xiao, P. F., Li, H. Wang, J. G. & Li, Y. (2012). Comparison of Snow Indexes in Estimating Snow Cover Fraction in a Mountainous Area in Northwestern China. IEEE Geoscience and Remote Sensing Letters, 9, 725-729.

Nagajothi, M., Priya G. & Sharma, P. (2019). Snow Cover Estimation of Western Himalayas using Sentinel-2 High Spatial Resolution Data. Indian Journal of Ecology, 46, 88-93.

O'Shaughnessy, S. A., Evett, S.R., Colaizzi, P. D., Andrade, M. A., Marek, T. H., Heeren, D. M., Lamm, F. R. & LaRue, J. L. (2019). Identifying Advantages and Disadvantages of Variable Rate Irrigation: An Updated Review. Applied Engineering in Agriculture, 35, 837–852.

Sharma, V. Mishra, V. D. & Joshi, P. K. (2012). Snow cover variation and streamflow simulation in a snow-fed river basin of the Northwest Himalaya. Journal of Mountain Science, 9, 853-868.

Shimamura, Y. Izumi, T. & Matsuyama, H. (2006). Evaluation of a useful method to identify snow-covered areas under vegetation - comparisons among a newly proposed snow index, normalized difference snow index, and visible reflectance. International Journal of Remote Sensing, 27, 4867-4884.

Smith, R., Oyler, L., Campbell, C., Woolley, E. A., Hopkins, B. G., Kerry, R. & Hansen, N. C. (2021). A new approach for estimating and delineating within-field crop water stress zones with satellite imagery, International Journal of Remote Sensing, 42, 6005-6024.

Svedin, J.D.; Kerry, R.; Hansen, N.C. & Hopkins, B.G. (2021). Identifying within-field spatial and temporal crop water stress to conserve irrigation resources with variable-rate Irrigation. Agronomy, 11, 1377.

Tisseyre, B., & McBratney, A. B. (2008). A technical opportunity index based on mathematical morphology for site-specific management: An application to viticulture. Precision Agriculture, 9, 101–113.

Woolley, E. A., Kerry, R., Hansen, N. C. & Hopkins, B. G. 2021. Variable rate irrigation: investigating within zone variability. *European Conference of Precision Agriculture,* Budapest, Hungary. July 2021. pp. 635-641.

Zhang, H. B., Zhang, F, Zhang, G. Q., Yan, W. & Li, S. E. (2021) Enhanced scaling effects significantly lower the ability of MODIS normalized difference snow index to estimate fractional and binary snow cover on the Tibetan Plateau. Journal of Hydrology, 592.